this family of domains mediates a host of biological processes, including protein internalization and signaling.


**References and Notes**

1. T. Pawson and J. D. Scott, *Science* **278**, 2075 (1997).
2. F. Fazioli, L. Minichiello, B. Matoskova, W. T. Wong, P. P. Di Fiore, *Mol. Cell. Biol.* **13**, 5814 (1993); W. T. Wong *et al.*, *Proc. Natl. Acad. Sci. U.S.A.* **92**, 9530 (1995).
3. A. E. Salcini *et al.*, *Genes Dev.* **11**, 2239 (1997).
4. M. Yamabhai *et al.*, in preparation.
5. B. Wendland and S. D. Emr, *J. Cell. Biol.* **141**, 71 (1998).
6. C. Haffner *et al.*, *FEBS Lett.* **419**, 175 (1997).
7. R. Carbone *et al.*, *Cancer Res.* **57**, 5498 (1997); A. Benmerah *et al.*, *J. Cell. Biol.* **140**, 1055 (1998).
8. H. S. Benedetti, F. Paths, F. Crausaz, H. Riezman, *Mol. Biol. Cell.* **5**, 1023 (1994); B. Wendland, J. M. McCaffery, Q. Xiao, S. D. Emr, *J. Cell Biol.* **135**, 1485 (1996).
9. A. Yamaguchi, T. Urano, T. Goi, L. A. Feig, *J. Biol. Chem.* **272**, 31230 (1997); M. Ikeda, O. Ishida, T. Hinoi, S. Kishida, A. Kikuchi, *ibid.* **273**, 814 (1998).
10. C. Schumacher *et al.*, *J. Biol. Chem.* **270**, 15341 (1995).
11. P. P. Di Fiore, P. G. Pelicci, A. Sorkin, *Trends Biochem. Sci.* **22**, 411 (1997).
12. A. Benmerah, B. Begue, A. Dautry-Varsat, N. Cerf-Bensussan, *J. Biol. Chem.* **271**, 12111 (1996).
13. F. Tebar, S. Confalonieri, R. E. Carter, P. P. Di Fiore, A. Sorkin, *ibid.* **272**, 15413 (1997); P. Cupers, E. ter Haar, W. Boll, T. Kirchhausen, *ibid.* **273**, 1847 (1998).
14. V. Avantaggiato, A. Torino, W. T. Wong, P. P. Di Fiore, A. Simeone, *Oncogene* **11**, 1191 (1995).
15. D. Rogaia *et al.*, *Cancer Res.* **57**, 799 (1997).
16. A DNA fragment encoding amino acids 121 through 218 of human Eps15 followed by a TAA stop codon was cloned into the Bam HI and Xho I sites of the pRSETA vector (Clontech). $Trp^{169} \rightarrow Ala^{169}$ and $Trp^{169} \rightarrow Tyr^{169}$ mutations were created by site-directed mutagenesis with the use of the Quickchange system (Stratagene) and were verified by dideoxysequencing. Wild-type $EH_2$ and mutants were transformed into *Escherichia coli* strains BL21 pLys S and B834 pLys S. Unlabeled or uniformly isotope labeled protein was obtained with LB broth or M9-minimal media containing $^{15}NH_4Cl$ and $^{13}C_6$-glucose. $His_6$-tagged $EH_2$ was purified with Talon resin (Clontech) and cleaved with Enterokinase (Novagen), followed by protease removal with EKapture agarose (Novagen). A matrix-assisted laser desorption ionization (MALDI) experiment of imidazole-eluted $His_6$-tagged $EH_2$ confirmed the size of 15.45 kD. Amino-terminal sequencing indicated that about 50% of $EH_2$ lacks the first two amino acids (encoded by the vector), which does not influence the folded structure. $EH_2$ is monomeric as determined by equilibrium sedimentation ultracentrifugation and pulsed field gradient diffusion experiments [A. S. Altieri, D. P. Hinton, R. A. Byrd, *J. Am. Chem. Soc.* **117**, 7566 (1995)]. All NMR spectra were recorded on samples containing 1 to 4 mM $EH_2$, 20 mM perdeuterated tris, 0.1 M KCl, 2 mM $CaCl_2$, 0.1 mM perdeuterated dithiothreitol, 10 μM 4-amidinophenylmethane sulfonyl fluoride, and 2 mM $NaN_3$ (pH = 7.0) dissolved in either 5 or 99.99% $^2H_2O/H_2O$. Calcium binding was assessed from NMR spectra of $EH_2$ in the presence of calcium and after addition of 10 mM EDTA. Even after repeated EDTA treatment at 37°C, approximately 20% of $EH_2$ still contained calcium (Fig. 3A). NMR experiments were recorded at 25°C on Varian INOVA 500-MHz and 600-MHz spectrometers equipped with shielded triple resonance probes. NMR experiments [D. R. Muhandiram and L. E. Kay, *J. Magn. Reson. B* **103**, 203 (1994); L. E. Kay, *Biochem. Cell. Biol.* **75**, 1 (1997)] were recorded essentially as described [M. Overduin, K. I. Tong, C. M. Kay, M. Ikura, *J. Biomol. NMR* **7**, 173 (1996)]. Spectra were analyzed with NMRPipe [F. Delaglio *et al.*, *ibid.* **6**, 277 (1995)] and in-house software on Sun Microsystems and Silicon Graphics workstations. Interproton distance restraints (313 intraresidue, 491 sequential, 509 short-range, and 432 long-range) were derived from three-dimensional (3D) and 4D isotope-filtered NOE spectra and were treated as described [C. M. Fletcher, D. N. M. Jones, R. Diamond, D. Neuhaus, *ibid.* **8**, 292 (1996)]. Dihedral restraints including 59 φ angles and 45 ψ angles were included based on $^3J_{HN-H\alpha}$ coupling constants and on $^1H\alpha$, $^{13}C\alpha$, and $^{13}C'$ chemical shifts [D. S. Wishart and B. D. Sykes, *ibid.* **4**, 171 (1994)]. Slowly exchanging amide protons were identified from several $^1H$-$^{15}N$ heteronuclear single quantum coherence (HSQC) spectra recorded over a week, after lyophilized protein was dissolved in 99.99% $^2H_2O$. In the final calculations, 20 pairs of hydrogen bond restraints were included and six distance restraints between calcium and coordinating oxygen atoms were added, based on average distances in EF hand proteins (*19*). Fifty structures were calculated with the $r^{-6}$ summation method in a restrained molecular dynamics simulated annealing protocol within X-PLOR 3.84 [A. Brünger, *X-PLOR, version 3.1* (Yale Univ. Press, New Haven, CT, 1992)]. Distance and dihedral angle restraints were treated with soft-square-well energy potentials and force constants of 50 kcal $mol^{-1}$ $Å^2$. The total, distance violation, and dihedral violation energies were 307 ± 12 kcal $mol^{-1}$, 57.0 ± 4.5 kcal $mol^{-1}$, and 0.68 ± 0.6 kcal $mol^{-1}$, respectively. No distance and angle restraints were violated by more than 0.35 Å and 2°, respectively. The rmsds from idealized geometry for bonds, angles, and impropers were 0.0028 ± 0.0001 Å, 0.62 ± 0.012°, and 0.47 ± 0.076°, respectively. Ramachandran plot analysis of the 20 structures with Procheck-NMR (*20*) showed that 85.8, 11.3, 2.5, and 0.5% of the non-Gly and non-Pro residues were in the most favorable, additional allowed, generously allowed, and disallowed regions, respectively.
17. Single-letter abbreviations for the amino acid residues are as follows: A, Ala; C, Cys; D, Asp; E, Glu; F, Phe; G, Gly; H, His; I, Ile; K, Lys; L, Leu; M, Met; N, Asn; P, Pro; Q, Gln; R, Arg; S, Ser; T, Thr; V, Val; W, Trp; and Y, Tyr.
18. Approximately 68 resonance units (RU) of $NH_2$-terminal biotinylated PTGSSSTNPFL (*17*) peptide (Research Genetics) were attached to a streptavidin-coated sensor chip in a BIAcore 2000 instrument. Wild-type $EH_2$ and the two $Trp^{169}$ mutants were injected over the peptide in eight concentrations ranging from 2 μm to 1.2 mM, with a flow rate of 30 μl $min^{-1}$ in 20 mM Pipes (pH 7.3), 50 mM KCl, 1 mM β-mercaptoethanol, 2 mM $CaCl_2$, 100 μM sodium azide, and 0.005% Tween-20. Equilibrium RU values were estimated at each protein concentration by averaging the steady-state response after injection and correcting for the sample refractive index component. The $K_D$ was estimated from the relation between the $EH_2$ concentration and equilibrium RU, using steady-state affinity analysis (BIAevaluation 2.1).
19. J. Falke, S. K. Drake, A. L. Hazard, O. B. Peersen, *Q. Rev. Biophys.* **27**, 219 (1994); R. Chattopadhyaya, W. E. Meador, A. R. Means, F. A. Quiocho, *J. Mol. Biol.* **228**, 1177 (1992); N. C. J. Strydnadka *et al.*, *ibid.* **273**, 238 (1997); J. P. Declerq, B. Tinant, J. Parello, J. Rambaud, *ibid.* **220**, 1017 (1991); L. A. Svensson, E. Thulin, S. Forsen, *ibid.* **223**, 601 (1992).
20. R. A. Laskowski, J. A. C. Rullmann, M. W. MacArthur, R. Kaptein, J. M. Thornton, *J. Biomol. NMR* **8**, 477 (1996).
21. Superposition of residues 121 through 215 yields rmsds of 0.54 ± 0.08 Å and 0.92 ± 0.10 Å for the backbone and all heavy atoms, respectively.
22. The disordered five $NH_2$-terminal residues [DRWGS (*17*)], which are encoded by the expression vector, and the six COOH-terminal residues, which are derived from the third EH domain (KTW) and expression vector (ELI), are not depicted.
23. A. Nicholls, K. A. Sharp, B. Honig, *Proteins* **11**, 281 (1991).


24. We thank R. Muhandiram and L. E. Kay for NMR pulse sequences, J. Mamay for computational support, S. A. Johnson for assistance with BIAcore experiments, P. P. Di Fiori for cDNA, B. Thimmig and C. McHenry for assistance with sedimentation equilibrium experiments, K. Clay and R. Murphy for MALDI data, and J. Enmon, D. Jones, and F. Tebar for insightful discussions. The NMR Center is supported by the Howard Hughes Medical Institute (HHMI). The University of Colorado Cancer Center Facilities for DNA and Protein Sequencing are supported by NIH. This research is funded by NIH and the HHMI (A.S. and M.O.) and by the American Cancer Society and Pew Scholar's Program (M.O.). T.B. and R.E.C. are recipients of NIH and Cancer League of Colorado postdoctoral fellowships, respectively. The coordinates have been deposited in the Brookhaven Protein Data Bank under accession number 1eh2.

30 April 1998; accepted 20 July 1998


# Direct Phosphorylation of IκB by IKKα and IKKβ: Discrimination Between Free and NF-κB–Bound Substrate


**Ebrahim Zandi,* Yi Chen,* Michael Karin†**



**A large protein complex mediates the phosphorylation of the inhibitor of κB (IκB), which results in the activation of nuclear factor κB (NF-κB). Two subunits of this complex, IκB kinase α (IKKα) and IκB kinase β (IKKβ), are required for NF-κB activation. Purified recombinant IKKα and IKKβ expressed in insect cells were used to demonstrate that each protein can directly phosphorylate IκB proteins. IKKα and IKKβ were found to form both homodimers and heterodimers. Both IKKα and IKKβ phosphorylated IκB bound to NF-κB more efficiently than they phosphorylated free IκB. This result explains how free IκB can accumulate in cells in which IKK is still active and thus can contribute to the termination of NF-κB activation.**


The IKK complex, isolated from extracts of HeLa cells treated with the proinflammatory cytokine TNF (tumor necrosis factor), phosphorylates two regulatory serine residues at the $NH_2$-termini of the NF-κB inhibitors IκBα and IκBβ (*1*). This phosphorylation event triggers the polyubiquitination of IκBs followed by their degradation through the

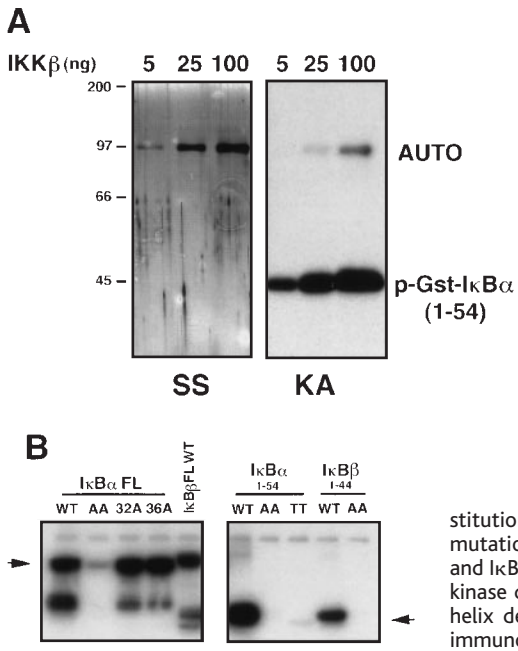


**Fig. 1.** Direct phosphorylation of IκB by IKKα and IKKβ. (**A**) IκBα phosphorylation by purified recombinant IKKβ. The protein was expressed using a baculovirus vector in Sf9 (*9*) cells and purified as described (*10*). The indicated amounts of highly purified IKKβ were separated by SDS-PAGE and visualized by silver staining (SS). These were also examined for phosphorylation of GST-IκBα(1–54) using a standard IκB kinase assay (KA). The phosphorylated GST-IκB(1–54) and IKKβ (Auto) bands are indicated. The migration positions of molecular size markers (in kilodaltons) are also indicated. Similar results were obtained for recombinant IKKα (*11*). (**B**) Substrate specificity of purified recombinant IKKβ was examined using GST-IκBα FL (full length) wild-type (WT), GST-IκBα FL with Ala at positions 32 and 36 (AA) or with single Ala substitutions at positions 32 (32A) or 36 (36A), GST-IκBβ FL, GST-IκBα(1–54) WT, GST-IκBα(1–54) AA, GST-IκBα(1–54) TT (Thr substitutions at positions 32 and 36), GST-IκBβ(1–44) WT, and GST-IκBβ(1–44) AA. (**C**) Effect of mutations on the kinase activities (KA) of recombinant IKKα and IKKβ. Autophosphorylation (Auto) and IκB kinase activities [with GST-IκBα(1–54) as a substrate] of purified recombinant wild type (WT), kinase defective [KM for IKKα and KA for IKKβ (*4*)], leucine zipper defective [LZ⁻ (*4*)], and helix-loop-helix defective [HLH⁻ (*4*)] mutants of IKKα and IKKβ, were determined. The bottom panels show immunoblots (IB) using anti-HA to detect WT IKKα and its derivatives (left) and anti-FLAG (M2) to detect WT IKKβ and its derivatives. (**D**) Phosphorylation of IκBα by different protein kinases. Wild-type GST-IκBα FL and GST-IκBα(A32/36) were incubated with similar amounts of the indicated protein kinases in standard kinase buffer and [$\gamma$-$^{32}$P]ATP for 30 min. The reactions were terminated and separated by SDS-PAGE, and the extent of substrate phosphorylation was revealed by autoradiography. The bands corresponding to the autophosphorylated kinases are indicated by a dot.

26*S* proteasome, and thereby leads to NF-κB activation (*2*). IKK is a large, 900-kD, protein complex that is composed of multiple subunits. Two of these subunits, IKKα and IKKβ, are serine kinases (*1, 3–6*). Epitope-tagged IKKα and IKKβ, when produced by cell-free translation in reticulocyte lysates or by transient transfection of mammalian cells, are incorporated into the IKK complex, which can be isolated by immunoprecipitation of either IKKα or IKKβ (*1, 4*). The IκB kinase activity of the entire complex is rapidly stimulated by TNF or interleukin 1 (IL-1), with kinetics matching those of IκBα phosphorylation and degradation (*1, 4*).

Because expression and immunoprecipitation of catalytically inactive IKKα or IKKβ mutants still resulted in isolation of a cytokine-inducible IκB kinase activity (*4*), the question was raised as to whether IKKα and IKKβ are directly responsible for IκB phosphorylation (*7*). Indeed, no IκB kinase activity was obtained after translation of IKKα or IKKβ in wheat germ extracts or after expression in *Escherichia coli* (*1, 4, 8*). Although transient expression of catalytically inactive IKKα or IKKβ mutants inhibits NF-κB activation (*1, 3–6*), these results are entirely compatible with IKKα and IKKβ being upstream kinases that activate another subunit of the IKK complex, which in turn phosphorylates IκB (*7*).

We used a baculovirus expression system to express $(His)_6$-HA–tagged IKKα and $(His)_6$-FLAG–tagged IKKβ separately or together in Sf9 insect cells (*9*). Recombinant IKKα and IKKβ were purified to apparent homogeneity from baculovirus-infected in-

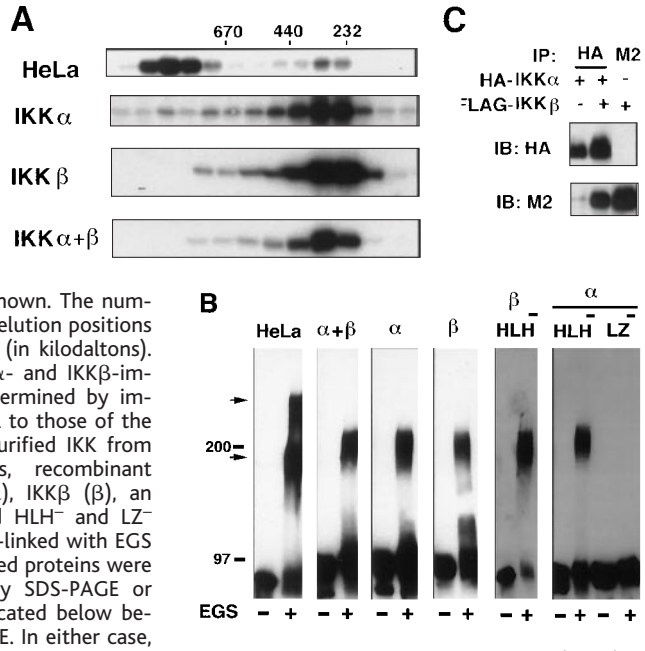


**Fig. 2.** Formation of dimers by IKKα and IKKβ. (**A**) The Superose 6 elution profile of the purified IKK complex from TNF-α–treated HeLa cells was compared to the elution profiles of purified recombinant IKKα, IKKβ, and IKKα-IKKβ (α+β) expressed in Sf9 cells (*1, 4*). The kinase activities toward GST-IκBα(1–54) are shown. The numbers at the top indicate the elution positions of molecular size standards (in kilodaltons). The elution profiles of IKKα- and IKKβ-immunoreactive materials determined by immunoblotting were identical to those of the kinase activities (*11*). (**B**) Purified IKK from TNF-α–treated HeLa cells, recombinant IKKα-IKKβ (α+β), IKKα (α), IKKβ (β), an HLH⁻ mutant of IKKβ, and HLH⁻ and LZ⁻ mutants of IKKα were cross-linked with EGS as described (*13*). Cross-linked proteins were either directly separated by SDS-PAGE or immunoprecipitated as indicated below before separation by SDS-PAGE. In either case, proteins were detected by immunoblotting. For the IKK complex from HeLa cells (HeLa), a representative blot shows an immunoblot (with anti-IKKα) of proteins that were immunoprecipitated with anti-IKKβ. An identical pattern of bands was observed when the blot was stripped and reprobed with anti-IKKβ (*13*). For the (HA)-IKKα–(FLAG)-IKKβ complex (α+β), the cross-linked proteins were immunoprecipitated with anti-HA and immunoblotted with anti-FLAG (M2). For (HA)-IKKα (α), (FLAG)-IKKβ (β), and the various mutants, the cross-linked proteins were directly resolved by SDS-PAGE and probed with anti-HA for IKKα and anti-FLAG (M2) for IKKβ. (**C**) Association of (HA)-IKKα and (FLAG)-IKKβ in coinfected Sf9 cells. (HA)-IKKα and (FLAG)-IKKβ were expressed either separately or together as indicated. The antibodies used for immunoprecipitation (IP) and immunoblotting (IB) were anti-HA and anti-FLAG (M2), as indicated.

Laboratory of Gene Regulation and Signal Transduction, Department of Pharmacology, University of California at San Diego, 9500 Gilman Drive, La Jolla, CA 92093, USA.

*These authors contributed equally to this report.
†To whom correspondence should be addressed. E-mail: karinoffice@ucsd.edu

sect cells (*10*). These purified proteins (Fig. 1A) (*11*) phosphorylated IκBα specifically on $Ser^{32}$ and $Ser^{36}$ and IκBβ on $Ser^{19}$ and $Ser^{23}$ (Fig. 1B) (*11*). Mutants of the $NH_2$-terminal regulatory domains of both IκBs in which threonine was substituted for these serine residues were not phosphorylated (Fig. 1B) (*11*). Mutants of IKKα and IKKβ that are defective in generation of IKK activity in mammalian cells (*4*) were also expressed in Sf9 cells and purified. These mutants showed little or no IκB kinase activity (Fig. 1C). Hence, IKKα and IKKβ appear to be direct IκB kinases. Comparison of purified IKKβ to a panel of seven other kinases indicated that it was the only kinase that specifically phosphorylated IκBα at $Ser^{32}$ and $Ser^{36}$, as revealed by the differences in $^{32}P$ incorporation into wild-type IκBα and the IκBα(A32/36) mutant (Fig. 1D). Even though some protein kinases such as casein kinase II (CKII) are efficient IκB kinases, the sites they phosphorylate are located in the COOH-terminal domain and not in the $NH_2$-terminal regulatory domain (*12*).

Recombinant IKKα and IKKβ expressed alone or together (IKKα-IKKβ) migrated on a Superose 6 gel filtration column with an apparent molecular size of 230 to 250 kD (Fig. 2A). The native IKK complex from HeLa cells has an apparent size of 900 kD (*1*). Thus, the Sf9 cells may lack components that are present in the large IKK complex. Chemical cross-linking (*13*) of recombinant IKKα, IKKβ, or IKKα-IKKβ complexes resulted in appearance of a single species migrating around 200 kD (Fig. 2B). Mutations in the leucine zipper (LZ) motif of IKKα abolished formation of the dimeric 200-kD cross-linked species (Fig. 2B). This mutant does not phosphorylate IκB proteins, indicating that dimerization of IKKα may be necessary for formation of a functional IκB kinase. Mutations in the helix-loop-helix (HLH) motifs of IKKα or IKKβ did not abolish their homodimerization, as judged by the appearance of the 200-kD cross-linked species (Fig. 2B). However, these mutations did result in loss of kinase activity (Fig. 1C). Thus, the HLH motifs of IKKα and IKKβ are necessary for catalytic activity even in the absence of other regulatory proteins.

Immunoprecipitation experiments with HA-tagged IKKα and FLAG-tagged IKKβ revealed formation of stable heterodimers when the two proteins were expressed together in Sf9 cells (Fig. 2C). We examined whether heterodimers in which one subunit was catalytically inactive would still catalyze the phosphorylation of IκBα (Fig. 3). Complexes of catalytically inactive IKKα and wild-type IKKβ exhibited similar IκB kinase activity to that of wild-type IKKα-IKKβ heterodimers. A heterodimer composed of wild-type IKKα and catalytically inactive IKKβ was also active, albeit not as active as wild-type IKKα homodimer. These results explain why immunoprecipitation of catalytically inactive IKKα or IKKβ transiently expressed in cultured mammalian cells results in formation of partially active IKK complexes (*4*).

IKKβ phosphorylated a fusion protein of glutathione transferase with the first 54 amino acids of IκB [GST-IκBα(1–54)] more efficiently than did IKKα (Fig. 4). However, full-length IκBα is phosphorylated by IKKα and IKKβ with similar efficiencies. The Michaelis constants ($K_m$) of IKKα and IKKβ toward full-length GST-IκBα were 2.1 and 2.2 μM, respectively (*14*).

In resting cells, cytoplasmic IκB proteins are associated with NF-κB dimers, and phosphorylation does not result in dissociation of this complex (*2*). Thus, the actual substrate for IKK is the IκB–NF-κB complex rather than free IκB. Some stimuli—such as IL-1, which is one of the strongest NF-κB activators—lead to prolonged activation of IKK that lasts 2 hours or more (*4*). Once IκBα is phosphorylated and degraded (within 3 to 10 min), NF-κB translocates to the nucleus and activates gene transcription (*15*), including that of the IκBα gene (*16*). Newly synthesized free IκBα accumulates within 60 min of the initial stimulus and translocates to the nucleus, where it binds DNA-bound NF-κB to induce its shuttling to the cytoplasm (*17*). This process is important for termination of the NF-κB response. But given the prolonged activation of IKK, it is puzzling how newly synthesized IκBα escapes the IKK-induced degradation pathway. We therefore compared the efficiency with which IKK phosphorylated free and NF-κB–bound IκBα (*18*). At similar concentrations, IκBα complexed with NF-κB was a better substrate for IKKα or IKKβ than was free IκBα (Fig. 5). Kinetic analysis indicated that in the presence of NF-κB, the $K_m$ for IκBα phosphorylation by IKKβ decreased from 2.2 μM to 1.4 μM and the relative maximum initial velocity $V_{max}$ was increased by a factor of 5 (*14*). Although IκBβ is not involved in rapid feedback inhibition of NF-κB activity (*19*), its phosphorylation by IKKα or IKKβ was also strongly enhanced by binding of NF-κB (Fig. 5). These results, which show that IKK prefers NF-κB–bound IκB proteins, explain why newly synthesized free IκBα is not phosphorylated and degraded in cells in which

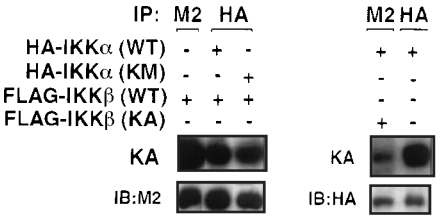


**Fig. 3.** Kinase activity of IKK heterodimers. Wild-type (FLAG)-IKKβ was expressed together with either wild-type (HA)-IKKα or kinase-defective (HA)-IKKα (KM) in Sf9 cells. Wild-type IKKα was expressed by itself or together with kinase-defective FLAG-IKKβ (KA). Extracts of cells infected with various combinations of the corresponding viruses, as indicated, were subjected to immunoprecipitation (IP) with either anti-HA or anti-FLAG (M2) as indicated. The kinase activity (KA) of each immune complex was examined with GST-IκBα(1–54) as a substrate. Amounts of wild-type (FLAG)-IKKβ or (HA)-IKKα proteins in the immune complexes were determined by immunoblotting (IB) with anti-FLAG (M2) or anti-HA, respectively. Exposure times for left and right panels were 1.5 and 5 hours, respectively.

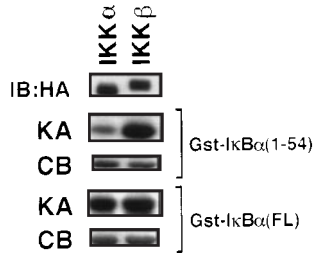


**Fig. 4.** Kinase activities of recombinant IKKα and IKKβ. (HA)-IKKα and (HA)-IKKβ were expressed separately in Sf9 cells (*10*) and immunoaffinity-purified on immobilized anti-HA. Immunoblot (IB) analysis shows that similar amounts of each protein were used to compare their kinase activities (KA) toward purified GST-IκBα(1–54) and GST-IκBα(FL) (full length). Coomassie blue (CB)–stained gels show the relative amounts of the two substrates.

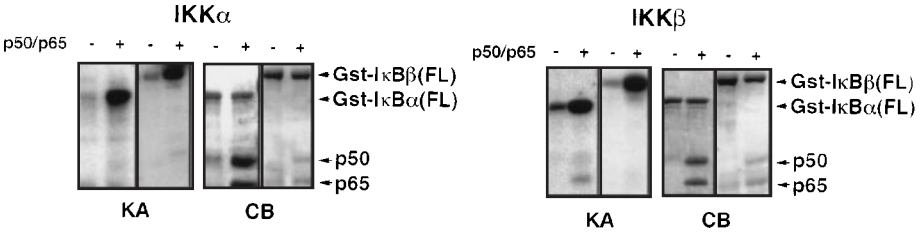


**Fig. 5.** Preferred phosphorylation by IKKs of IκBs bound to NF-κB. The kinase activities (KA) of purified (HA)-IKKα (left panel) or (FLAG)-IKKβ (right panel) toward free or NF-κB–prebound GST-IκBα(FL) and GST-IκBβ(FL) were measured. The NF-κB heterodimer was composed of recombinant p50 and the Rel homology domain of p65 (*18*). Shown are the autoradiograms of the kinase assays (KA) and Coomassie blue (CB)–stained gels depicting the various substrates.

IKK remains active after the initial inductive stimulus.

The IKKα and IKKβ protein kinases, and not another component of the IKK complex, appear to be directly responsible for IκB phosphorylation. The minimal active IKK complex is apparently a dimer composed of IKKα or IKKβ (or both). These experiments also provide an explanation for the mechanism underlying the termination of the NF-κB activation response. Such inactivation is important because prolonged or chronic NF-κB activation can result in inflammatory disorders (*20*).

**References and Notes**


1. J. A. DiDonato, M. Hayakawa, D. M. Rothwarf, E. Zandi, M. Karin, *Nature* **388**, 548 (1997).
2. I. Alkalay *et al.*, *Mol. Cell. Biol.* **15**, 1294 (1995); J. A. Brockman *et al.*, *ibid.*, p. 2809; K. Brown, S. Gerstberger, L. Carlson, G. Franzoso, U. Siebenlist, *Science* **267**, 1485 (1995); Z. Chen *et al.*, *Genes Dev.* **9**, 1586 (1995); J. A. DiDonato, F. Mercurio, M. Karin, *Mol. Cell. Biol.* **15**, 1302 (1995); E. B. M. Traenckner *et al.*, *EMBO J.* **14**, 2876 (1995); S. T. Whiteside *et al.*, *Mol. Cell. Biol.* **15**, 5339 (1995); J. A. DiDonato *et al.*, *ibid.* **16**, 1295 (1996).
3. C. H. Regnier, H. Yeong Song, X. Gao, D. V. Goeddel, *Cell* **90**, 373 (1997).
4. E. Zandi, D. M. Rothwarf, M. Delhase, M. Hayakawa, M. Karin, *ibid.* **91**, 243 (1997).
5. F. Mercurio *et al.*, *Science* **278**, 860 (1997).
6. J. D. Woronicz, X. Gao, Z. Cao, M. Rothe, D. V. Goeddel, *ibid.*, p. 866.
7. I. Stancovski and D. Baltimore, *Cell* **91**, 299 (1997).
8. E. Zandi, D. Rothwarf, J. DiDonato, unpublished results.
9. Transfer vectors were constructed using the baculovirus transfer vector pAcSGHis NT-B (Pharmingen). All inserts were prepared by polymerase chain reaction (PCR). HA-tagged IKKα (the HA epitope is fused in frame to the second amino acid of IKKα) was generated by PCR using the primers 5′-TACTAGCTCGAGGATACCCTTACGATGTTCCTGATTACGCTGAGCGGCCCCCGGGG-3′ and 5′-AGCTATCGCGGCCGCTCATTGTGTTAACCAAC-3′. This fragment was digested with Xho I and Not I and cloned into the corresponding sites of pAcSGHis NT-B. In the resulting vector, the $(His)_6$ tag is upstream of and in frame with the HA epitope. A similar strategy was used to generate the transfer vectors for $(His)_6$-HA–IKKβ and $(His)_6$-FLAG–IKKβ. Primers for FLAG-tagged and HA-tagged IKKβ were 5′-AGCTATCGCGGCCGCGACTACAAGGACGACGATGACAAAAGCTGGTCACCTTCC-3′, 5′-AGCTAGCGCGGCCGCTACCCTTACGATGTTCCTGATTACGCTAGCTGGTCACCTTCC-3′, and 5′-TGACTCCCGGGTCATGAGGCCTGCTCC-3′. For the generation of recombinant viruses, we followed the manufacturer's (Pharmingen) recommendations for growth and maintenance of Sf9 cells, preparation of recombinant baculoviruses, and infection of the cells. For in vivo recombination, we transfected the transfer vectors and BaculoGold DNA into Sf9 cells using SuperFect (Qiagen). To prepare a control viral stock, we cotransfected Sf9 cells with unmodified pAcSGHis NT-B vector and BaculoGold DNA. After 5 days, culture supernatants were collected and amplified by two rounds of infection. For expression of both IKKα and IKKβ, the corresponding recombinant viruses were mixed in various ratios before infection of Sf9 cells. The efficiency of infection was determined by indirect double immunofluorescence using antibodies to HA and FLAG.
10. Recombinant $(His)_6$-HA–IKKα and $(His)_6$-FLAG–IKKβ proteins were produced in Sf9 cells after infection with high-titer recombinant viruses. The proteins were purified as described (*1*). Briefly, cell extracts were fractionated on Q-Sepharose and the fractions containing IKK were applied to an adenosine triphosphate (ATP) affinity column. Bound proteins were eluted with 20 mM ATP and applied to a Superose 6 gel filtration column. The fractions containing IKK (200 to 250 kD range) were then bound to Ni-Sepharose and washed extensively with AP buffer (500 mM NaCl, 1% Triton X-100, and 2 M urea) (*1*) and eluted with 200 mM imidazole. The eluted IKKs were either separated by SDS–polyacrylamide gel electrophoresis (PAGE) (8% gel) and visualized by silver staining or further purified by immunoaffinity chromatography with anti-FLAG (M2)–coupled Sepharose for IKKβ or anti-HA–coupled Sepharose for IKKα.
11. E. Zandi and Y. Chen, unpublished results. IKKα does not discriminate between full-length wild-type IκBα and the IκBα(A32/36) mutant as effectively as does IKKβ. In addition to $Ser^{32}$ and $Ser^{36}$, IKKα and to a lesser extent IKKβ also phosphorylate sites close to the COOH-terminus of IκBα (*1*).
12. C. F. Barroga, J. K. Stevenson, E. M. Schwarz, I. M. Verma, *Proc. Natl. Acad. Sci. U.S.A.* **92**, 7637 (1995); J. A. McElhinny, S. A. Trushin, G. D. Bren, N. Chester, C. V. Paya, *Mol. Cell. Biol.* **16**, 899 (1996); E. M. Schwarz, D. VanAntwerp, I. M. Verma, *ibid.*, p. 3554.
13. Purified IKK proteins were cross-linked in the presence of bovine serum albumin (BSA, 1 mg/ml) in AP buffer containing 300 mM NaCl, 1% Triton X-100, and 2 mM ethylene glycol-*bis*(succinimidylsuccinate) (EGS; Pierce) for 20 min at room temperature. The cross-linker was inactivated by addition of 500 mM tris-HCl (pH 8.0). Cross-linked proteins were either immunoprecipitated (as described below) before separation by SDS-PAGE (4.5% gel) or directly subjected to SDS-PAGE. Proteins were visualized by immunoblotting with specific antibodies. For immunoprecipitation, the cross-linked IKK preparations were divided in two; one portion was immunoprecipitated with anti-IKKα and the other with anti-IKKβ. The immune complexes were separated by SDS-PAGE (4.5% gel) and proteins were transferred to a membrane and immunoblotted with an antibody to the other subunit than the one used for immunoprecipitation.
14. Various amounts of GST-IκBα (full-length) or GST-IκBα(1–54) were incubated with purified $(His)_6$-HA–IKKα or $(His)_6$-FLAG–IKKβ in kinase assay buffer (*1*) with 200 μM [$\gamma$-$^{32}$P]ATP for 20 min at 30°C. The reactions were stopped by adding SDS loading buffer, and proteins were resolved by SDS-PAGE (10% gel). The phosphorylated IκB bands were visualized and quantified by a phosphoimager (Bio-Rad). The amount of radioactivity in each band was plotted against the substrate concentration using a nonlinear regression program (SigmaPlot). The $K_m$ values for each enzyme were determined from the corresponding plots.
15. For a review, see I. M. Verma *et al.*, *Genes Dev.* **9**, 2723 (1995).
16. S. C. Sun, P. A. Ganchi, D. W. Ballard, W. C. Greene, *Science* **259**, 1912 (1993).
17. F. Arenzana-Seisdedos *et al.*, *Mol. Cell. Biol.* **15**, 2689 (1995).
18. Full-length GST-IκBα or GST-IκBβ (2 μg) were incubated with an excess of purified NF-κB dimers formed from recombinant p50(NF-κB1) and the Rel homology domain of p65(RelA) [F. E. Chen, D. B. Huang, Y. Q. Chen, G. Ghosh, *Nature* **391**, 410 (1998)]. The GST-IκB-p50-p65 complexes were separated from free NF-κB by chromatography on glutathione–Sepharose 4B (Pharmacia). The ternary IκB–NF-κB complexes, whose formation was confirmed by SDS-PAGE and Coomassie blue staining, were washed with kinase buffer before kinase assay.
19. J. E. Thompson, R. J. Philips, H. Erdjument-Bromage, P. Tempst, S. Ghosh, *Cell* **80**, 573 (1995).
20. P. J. Barnes and M. Karin, *N. Engl. J. Med.* **336**, 1066 (1997).


21. We thank D. Rothwarf and F. Mercurio for insightful discussions and reagents; Z. Radic for help with kinetic analysis; G. Ghosh for purified NF-κB proteins (*18*); G. Cadwell for excellent technical assistance; and B. Thompson for help with manuscript preparation. E.Z. was supported by a junior postdoctoral fellowship from the American Cancer Society. Supported by NIH grant AI 43477 (M.K.).

19 May 1998; accepted 20 July 1998


# Optimizing Gaze Control in Three Dimensions


**Douglas Tweed,*† Thomas Haslwanter, Michael Fetter**



**Horizontal and vertical movements of the human eye bring new objects to the center of the visual field, but torsional movements rotate the visual world about its center. Ocular torsion stays near zero during head-fixed gaze shifts, and eye movements to visual targets are thought to be driven by purely horizontal and vertical commands. Here, analysis of eye-head gaze shifts revealed that gaze commands were three-dimensional, with a separate neural control system for torsion. Active torsion optimized gaze control as no two-dimensional system could have, stabilizing the retinal image as quickly as possible when it would otherwise have spun around the fixation point.**


The human eye rotates with three degrees of freedom: horizontally, vertically, and torsionally (*1*, *2*). With few exceptions, theories of vision and eye movement have ignored rotations about the line of sight. One reason is Listing's law (*1*, *3*, *4*), which states that ocular torsion stays near zero during head-fixed gaze shifts. This has been taken as confirmation that gaze is driven by purely horizontal and vertical commands. Here we show that Listing's law is just one mode of gaze control, valid only when the head is stationary.

When eye and head join forces to transport the gaze line, the logistics are complex. For one thing, the eye is quicker than the head—it reorients more swiftly when an interesting object


D. Tweed, Departments of Physiology and Applied Mathematics, University of Western Ontario, London, Canada. T. Haslwanter and M. Fetter, Department of Neurology, University of Tübingen, Germany.

*Present address: Department of Physiology, Medical Sciences Building 3207, University of Toronto, 1 King's College Circle, Toronto, Ontario, M5S 1A8, Canada.

†To whom correspondence should be addressed.